Computationally Efficient Fail-safe Trajectory Planning for Self-driving Vehicles Using Convex Optimization

Christian Pek[1] and Matthias Althoff[2]

Abstract—Ensuring the safety of self-driving vehicles is a challenging task, especially if other traffic participants severely deviate from the predicted behavior. One solution is to ensure that the vehicle is able to execute a collision-free evasive trajectory at any time. However, a fast method to plan these so-called fail-safe trajectories does not yet exist. Our new approach plans fail-safe trajectories in arbitrary traffic scenarios by incorporating convex optimization techniques. By integrating safety verification in the planner, we are able to generate fail-safe trajectories in real-time, which are guaranteed to be safe. At the same time, we minimize jerk to provide enhanced comfort for passengers. The proposed benefits are demonstrated in different urban and highway scenarios using the CommonRoad benchmark suite and compared to a widely-used sampling-based planner.

I. INTRODUCTION

The development of self-driving vehicles promises enhanced road safety. However, after test vehicles have encountered their first accidents, multiple institutions around the world have raised concerns about safe motion planning [1]. Various concepts aiming to guarantee safety in arbitrary traffic situations have been proposed (cf. Sec. I-A).

An interesting approach is the fail-safe planning framework proposed in [2] (cf. general idea in Fig. 1). This framework enforces the existence of a fail-safe trajectory, which is collision-free with respect to any legal future motion of obstacles, at any time. If traffic participants violate certain traffic rules, the approach adjusts and also considers behaviors ignoring traffic rules. If traffic participants deviate from the predicted motion, the vehicle has two options to remain safe: (1) execute the previously computed fail-safe trajectory (cf. Fig. 1a), or (2) find a new combination of an intended motion and fail-safe trajectory (cf. Fig. 1b). The concept in [2] only specifies safety properties, but does not propose a method to compute fail-safe trajectories in arbitrary scenarios with low computational costs, which is addressed in this work.

A. Literature Overview

a) Trajectory planning: Various trajectory planning approaches are discussed in [3]. We briefly review the most popular below. Sampling-based planners, such as *rapidly exploring random trees* [4]–[6], randomly sample and connect collision-free states toward a specified goal region to obtain

[1]Christian Pek is with the Department of Computer Science, Technical University of Munich, D-85748 Garching, Germany and BMW Group, D-85716 Unterschleißheim, Germany. `Christian.Pek@bmw.de`

[2]Matthias Althoff is with the Department of Computer Science, Technical University of Munich, D-85748 Garching, Germany `althoff@in.tum.de`

(a) Initial scenario
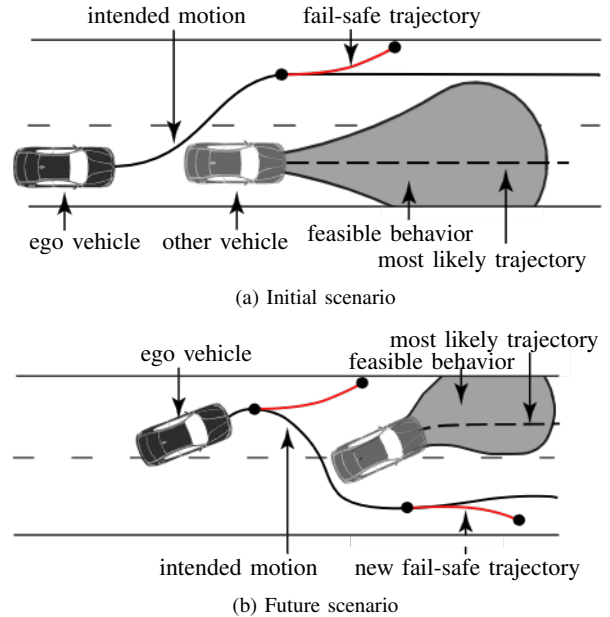

(b) Future scenario

Fig. 1: Fail-safe trajectories are collision-free with respect to any feasible behavior of obstacles (a). While the ego vehicle proceeds along its intended motion, new fail-safe trajectories are computed to ensure safety at any time (b). In case no new valid fail-safe trajectory is found, the previously computed fail-safe trajectory is executed.

kinematically feasible trajectories. However, the randomization step may lead to large computation times. Furthermore, sampling may cause motions with high jerks, which should be avoided in case the critical situation resolves, i.e., a new collision-free intended motion has been determined.

State lattices compute a trajectory set over a predefined and fixed grid of goal states. In combination with optimal control, state lattices can produce jerk-optimal trajectories [7]. However, predefined grids lead to non-optimal solutions.

Continuous optimization techniques are used to overcome discretization effects that limit sampling-based planners [8], [9]. Trajectories are obtained by minimizing a certain cost function subject to a set of state and input constraints despite disturbances. For example, mixed-integer programming is used in [10] and non-linear programming in [11]. Nevertheless, optimization may be harder to solve due to the non-convex nature of most motion planning problems [12].

Instead, convex approximations of motion planning problems can be used. Convex optimization offers the advantage of global convergence and the existence of mature and efficient solving techniques [13]–[15], which have been numerously applied to automotive problems, see e.g., [16]–

[20]. Nevertheless, in most traffic situations with multiple other vehicles, the planning problem can only be formulated as convex if the motion is separated into longitudinal and lateral components, possibly resulting in non-drivable solutions. However, we show that our approach can combine both motions while obtaining feasible trajectories, even in heavily linked situations such as evading.

As for planning evasive trajectories, most works focus on a discrete set of maneuvers, so that they can only handle specific traffic situations or cannot ensure safety if traffic participants deviate from the predicted motion [21]–[25].

b) Safety verification: In general, planned trajectories are only collision-free if obstacles do not deviate from the predicted motion used during planning. Reachability analysis [26] has been used to verify the safety of trajectories with respect to any feasible future motion of obstacles. This is done by computing the reachable set of obstacles, i.e., the set of reachable states from a given initial set, and checking for collisions with the trajectory of the ego vehicle [27]–[29]. However, if a trajectory is regarded as unsafe, no alternative trajectory to avoid a collision is returned.

Logical reasoning has also been applied to safety verification. For instance, lane change maneuvers are verified in [30], [31] and safe vehicle following is verified in [32]. Although these approaches guarantee safety, the logical formulas involved are often complex and adjusted to the considered traffic situation.

To ensure that trajectories with finite planning horizons remain safe beyond the planning horizon, trajectories must end in a safe state, e.g., by avoiding inevitable collision states [33], [34]. States of invariant sets guarantee the existence of at least one collision-free trajectory [35], [36].

Note that the focus of this work is not to check if planned fail-safe trajectories end in a safe state. However, such a goal region may be incorporated as a terminal constraint in our approach. Furthermore, we assume redundant hardware, allowing us to ignore hardware faults.

B. Contributions

This paper introduces a method to compute fail-safe trajectories in arbitrary traffic scenarios. Unlike existing work, our approach can

1) plan fail-safe trajectories in real-time by making use of convex optimization, in particular quadratic programming,
2) guarantee the safety of planned trajectories with respect to any feasible (legal) future motion of obstacles, and
3) enhance passenger comfort by minimizing jerks, which is beneficial if the critical situation resolves.

The remainder of this paper is structured as follows: In Sec. II, we introduce mathematical models and assumptions. The trajectory planners are described in Sec. III. Subsequently, the procedure for computing fail-safe trajectories is explained in Sec. IV. The benefits of the proposed concept are highlighted in different urban and highway scenarios and compared to a widely-used sampling-based trajectory planner in Sec. V. We finish with conclusions in Sec. VI.

II. PRELIMINARIES

Let us introduce the configuration space $\mathcal{X} \subset \mathbb{R}^n$ as the possible set of states x and $\mathcal{U} \subset \mathbb{R}^m$ as the set of admissible control inputs u of a self-driving vehicle, whose motion is governed by the differential equation

$$\dot{x}(t) = f\big(t, x(t), u(t), z(t)\big), \tag{1}$$

where $z(t) \in \mathcal{Z}$ describes disturbances. We use $x^{(i)}, i \in \mathbb{N}_0$ to describe the i-th component of the state variable x. Without loss of generality, we assume that the initial time is $t_0 = 0$, and we adhere to the notation $x([t_0, t_h])$ to describe a state trajectory for the time interval $[t_0, t_h], t_0 < t_h$.

We consider a lane-based environment for fail-safe planning, which is modeled as a subset of the Euclidean space $\mathbb{R}^k$. We introduce a relation occ from the configuration space $\mathcal{X}$ to the lane-based environment in world coordinates:

Definition 1 (Occupancy of States)
The operator $\mathrm{occ}(x)$ relates the state vector x to the set of points in the environment occupied by the system as $\mathrm{occ}(x) : \mathcal{X} \to \mathrm{P}(\mathbb{R}^k)$, where $\mathrm{P}(\mathbb{R}^k)$ is the power set of $\mathbb{R}^k$. Given a set $\mathcal{X}$, we define $\mathrm{occ}(\mathcal{X}) := \{\mathrm{occ}(x) \,|\, x \in \mathcal{X}\}$.

A curvilinear coordinate system is used for motion planning and is aligned to a given reference path Γ. This means that all Euclidean positions will be described in terms of the arclength s along Γ and the orthogonal deviation d to Γ (cf. Fig. 2).

The set $\mathcal{B} \subset \mathbb{N}_+$ contains indices, referring to all safety-relevant obstacles within the environment, e.g., obtained from on-board sensors of the vehicle [37]. In order to guarantee safety of planned motions, we assume the existence of a prediction which accounts for any feasible future motion of obstacles, see e.g., [38]. The set of possibly occupied points at a given point in time is represented as an occupancy set:

Definition 2 (Occupancy Set)
The occupancy set $\mathcal{O}(t) \subseteq \mathbb{R}^k$ describes the set of points in the environment possibly occupied by an obstacle at time t. For the time interval $[t_1, t_2], t_1 < t_2$, we define $\mathcal{O}([t_1, t_2]) = \bigcup_{t_1 \le t \le t_2} \mathcal{O}(t)$.

III. TRAJECTORY GENERATION

To reduce computational cost, we use a convex approximation of the motion planning problem [13]. This is achieved by separating motions into a longitudinal and a lateral component while guaranteeing the drivability of the resulting motion plan.

A. Longitudinal Motion

We model the state of the vehicle's longitudinal motion as $x_{\mathrm{lon}} = (s, v, a, j)^T$, where s is the longitudinal position, v is the velocity, a is the acceleration, and j is the jerk along a given reference path Γ (cf. Fig. 2). Using the input $u(t) = \dddot{a}(t)$, the longitudinal motion of the vehicle is represented by the linear time-invariant system

$$\frac{d^4}{dt^4} s(t) = u(t). \tag{2}$$

To ensure that the trajectory is kinematically feasible, the following time-invariant state constraints apply:

$$a_{\min} \leq a(t) \leq a_{\max},$$
$$v_{\min} \leq v(t) \leq v_{\max}. \tag{3}$$

For collision avoidance, positions are restricted based on obstacles blocking the reference path Γ:

$$s_{\min}(t) \leq s(t) \leq s_{\max}(t). \tag{4}$$

The quadratic cost function J_{lon} favors comfortable trajectories by punishing high accelerations and jerk with weights $w_a \in \mathbb{R}_+$ and $w_j \in \mathbb{R}_+$, respectively, and is defined as:

$$J_{\mathrm{lon}}\big(x_{\mathrm{lon}}(t)\big) = \int_0^{t_h} w_a x_{\mathrm{lon}}^{(2)}(t)^2 + w_j x_{\mathrm{lon}}^{(3)}(t)^2 \ dt. \tag{5}$$

B. Lateral Motion

The lateral motion of the vehicle is described by the state $x_{\mathrm{lat}} = (d, \theta, \kappa, \dot{\kappa})^T$, where d is the lateral distance to the reference path Γ, θ is the orientation, κ is the curvature, and $\dot{\kappa}$ is the change of curvature of the ego vehicle. In order to obtain smooth lateral motion profiles, we choose the input $u(t) = \ddot{\kappa}(t)$.

As the vehicle is supposed to move along the predefined reference path, we can assume that the difference $\Delta = \theta - \theta_\Gamma$ between the current orientation and the reference path orientation θ_Γ is negligibly small. Thus, the trigonometric functions can be approximated as $\sin(\Delta) \approx \Delta$ and $\cos(\Delta) \approx 1$. To efficiently integrate collision avoidance without introducing a new state variable, we model the orientation θ_Γ of the reference path Γ as a disturbance $z(t) = \theta_\Gamma\big(s(t)\big)$. Then, the lateral motion of the vehicle is given by the time-variant linear system

$$\dot{x}_{\mathrm{lat}} = \begin{pmatrix} 0 & v(t) & 0 & 0 \\ 0 & 0 & v(t) & 0 \\ 0 & 0 & 0 & 1 \\ 0 & 0 & 0 & 0 \end{pmatrix} x_{\mathrm{lat}}(t) + \begin{pmatrix} 0 \\ 0 \\ 0 \\ 1 \end{pmatrix} u(t) + \begin{pmatrix} -v(t) \\ 0 \\ 0 \\ 0 \end{pmatrix} z(t). \tag{6}$$

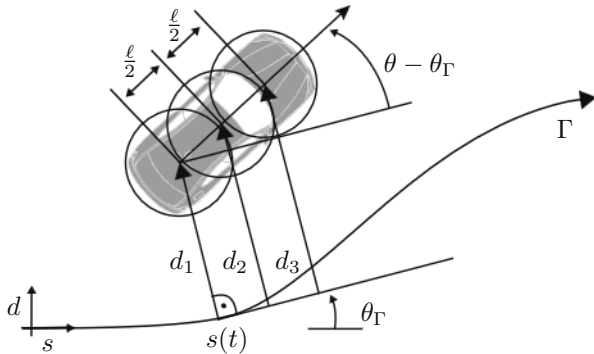Note that (6) qualifies as a linear system because $v(t)$ is not a state variable for the lateral dynamics.

Fig. 2: Kinematic model with respect to a curvilinear coordinate system aligned to the reference path Γ with orientation θ_Γ. The vehicle's pose is described by the longitudinal position s, the lateral deviation d, and the orientation θ.

For collision checking, we approximate the shape of the vehicle using three circles with equal radius r (cf. Fig. 2) [39]. Without loss of generality, we choose the centers of the first and third circle to coincide with the rear and front axle, respectively. The distance between the center points corresponds to ℓ. The center of the second circle is positioned such that the distance to the other circle's center is $\frac{1}{2}\ell$. Thus, the lateral distance d_i from the i-th circle's center, $i \in \{1, 2, 3\}$, to the reference path Γ is obtained as:

$$d_i = d + \frac{i-1}{2}\ell \sin(\theta - \theta_\Gamma) \approx d + \frac{i-1}{2}\ell(\theta - \theta_\Gamma). \tag{7}$$

We define the constrained values of the system as $x_{\mathrm{constr}} = (d_1, d_2, d_3, \kappa, \dot{\kappa})^T$:

$$x_{\mathrm{constr}}(t) = \begin{pmatrix} 1 & 0 & 0 & 0 \\ 1 & \frac{1}{2}\ell & 0 & 0 \\ 1 & \ell & 0 & 0 \\ 0 & 0 & 1 & 0 \\ 0 & 0 & 0 & 1 \end{pmatrix} x_{\mathrm{lat}}(t) + \begin{pmatrix} 0 \\ -\frac{1}{2}\ell \\ -\ell \\ 0 \\ 0 \end{pmatrix} z(t). \tag{8}$$

By computing the allowed minimum and maximum lateral displacement along the reference path Γ for each circle $i \in \{1, 2, 3\}$, we can incorporate collision avoidance constraints into the lateral motion model. Furthermore, the physical constraints of the steering actuators are included:

$$\underbrace{\begin{pmatrix} d_{1,\min}(t) \\ d_{2,\min}(t) \\ d_{3,\min}(t) \\ \kappa_{\min}(t) \\ \dot{\kappa}_{\min}(t) \end{pmatrix}}_{x_{\min}(t)} \leq x_{\mathrm{constr}}(t) \leq \underbrace{\begin{pmatrix} d_{1,\max}(t) \\ d_{2,\max}(t) \\ d_{3,\max}(t) \\ \kappa_{\max}(t) \\ \dot{\kappa}_{\max}(t) \end{pmatrix}}_{x_{\max}(t)}. \tag{9}$$

The quadratic cost function J_{lat} with weights $w_d \in \mathbb{R}_+, w_\theta \in \mathbb{R}_+, w_\kappa \in \mathbb{R}_+$, and $w_{\dot{\kappa}} \in \mathbb{R}_+$ minimizes the lateral distance to Γ and orientation deviation from θ_Γ and punishes high curvature rates to achieve smooth trajectories:

$$J_{\mathrm{lat}}\big(x_{\mathrm{lat}}(t)\big) = \int_0^{t_h} w_d x_{\mathrm{lat}}^{(0)}(t)^2 + w_\theta \big(x_{\mathrm{lat}}^{(1)}(t) - \theta_\Gamma(t)\big)^2$$
$$+ w_\kappa x_{\mathrm{lat}}^{(2)}(t)^2 + w_{\dot{\kappa}} x_{\mathrm{lat}}^{(3)}(t)^2 \ dt. \tag{10}$$

C. Categorization of the Optimization Problem

The vehicle models for both the longitudinal and lateral trajectory planning problems are linear. In addition, the input $u(t)$ and state $x(t)$ in (1) are subject to linear constraints:

$$u_{\min}(t) \leq u(t) \leq u_{\max}(t),$$
$$x_{\min}(t) \leq x(t) \leq x_{\max}(t). \tag{11}$$

The optimization problem for a quadratic cost function $J(x) : \mathbb{R}^n \times \mathbb{R}^m \to \mathbb{R}$ over the time horizon t_h

$$\operatorname*{argmin}_u \int_0^{t_h} J\big(x(t)\big) \ dt, \quad \textit{subject to: } (1), (11)$$

is a convex optimization problem [13, p. 152].

IV. COMPUTATION OF FAIL-SAFE TRAJECTORIES

Fig. 3 illustrates the procedure for computing fail-safe trajectories using the decoupled motion problems described in Sec. III. We assume that the initial state x_0 of the fail-safe trajectory and the reference path Γ to be known a priori. Note that computing Γ is not the focus of this work; readers are referred to [3, Sec. IV].

In Step 1 of Fig. 3, the longitudinal collision constraints are extracted. To accomplish this, we transform the predicted occupancy $\mathcal{O}_b(t)$ (cf. Def. 2) of each safety-relevant obstacle $b \in \mathcal{B}$ in a curvilinear coordinate system aligned with Γ, resulting in $\mathcal{O}_{b,\mathrm{cls}}(t)$. Based on the longitudinal position of the vehicle s_{ego}, the position constraint $s(t) \leq s_{\mathrm{max}}(t)$ in (4) is computed as (cf. Fig. 4):

$$s_{\mathrm{max}}(t) = \inf \left\{ s > s_{\mathrm{ego}} \mid (s, d)^T \in \mathcal{O}_{b,\mathrm{cls}}(t), b \in \mathcal{B} \right\}. \quad (12)$$

The minimum position constraint $s(t) \geq s_{\mathrm{min}}(t)$ is obtained similarly as:

$$s_{\mathrm{min}}(t) = \sup \left\{ s < s_{\mathrm{ego}} \mid (s, d)^T \in \mathcal{O}_{b,\mathrm{cls}}(t), b \in \mathcal{B} \right\}. \quad (13)$$

Note that $s_{\mathrm{min}}(t)$ is only used if the ego vehicle is changing to another lane as described in [40].

In Step 2, we check if a braking maneuver alone is sufficient to avoid a collision as this is often considered to be the most comfortable maneuver for passengers. Since the occupancy sets include information about the dynamics of the obstacles over time, we can use (12) for this check.

Proposition 1 (Collision Avoidance Through Braking)
A collision with obstacles, represented as a collision constraint $s(t) \leq s_{\mathrm{max}}(t), t \in [0, t_h]$, can be avoided for the
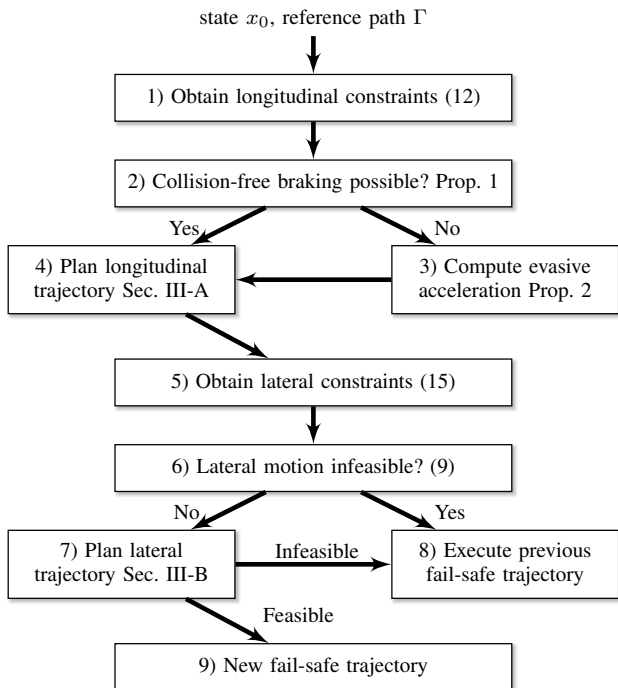

Fig. 3: Procedure for fail-safe trajectory computation with a given initial state x_0 and reference path Γ.
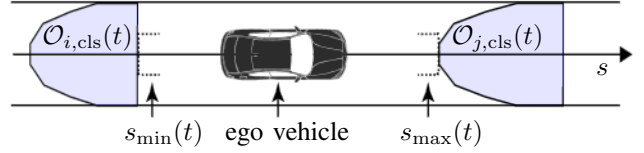

Fig. 4: Illustration of calculating the longitudinal collision constraints, s_{min} and s_{max}, in a lane for given occupancy sets $\mathcal{O}_{i,\mathrm{cls}}$ and $\mathcal{O}_{j,\mathrm{cls}}$.

initial position s_0, velocity v_0, and reaction time δ_{brake} of the vehicle using emergency braking with $|a_{\mathrm{max}}|$ if

$$\forall t \in [0, t_h] : s_0 + v_0(\tau + \delta_{\mathrm{brake}}) - \frac{1}{2}|a_{\mathrm{max}}|\tau^2 \leq s_{\mathrm{max}}(t),$$
$$\tau := \min(t, v_0/|a_{\mathrm{max}}|).$$

Proof: Using the maximum feasible deceleration a_{max}, collision-avoidance using braking directly follows from the definition of $s_{\mathrm{max}}(t)$ in (12). ∎

If the ego vehicle can avoid a potential collision using braking, the longitudinal trajectory is computed using the planner described in Sec. III-A. An example, in which the ego vehicle avoids a collision with crossing traffic by initiating a braking maneuver, is illustrated in Fig. 6b.

Otherwise, a collision may be avoided by swerving to another lane or evading obstacles without leaving the current lane. For these situations, let us first introduce the *guaranteed time-to-collision*.

Definition 3 (Guaranteed Time-To-Collision)
The guaranteed time-to-collision (GTTC) with respect to the initial longitudinal position s_0 and velocity v_0 of the vehicle and the maximum allowed position $s_{\mathrm{max}}(t), t \in [0, t_h]$ is defined as

$$\mathrm{GTTC} := \underset{t \in [0, t_h]}{\mathrm{argmin}} \left| (s_0 + v_0 t) - s_{\mathrm{max}}(t) \right|.$$

Due to the decoupled longitudinal and lateral dynamics in the vehicle motion model, we must ensure that the necessary maximum lateral acceleration a_{eva} for evading is feasible throughout the maneuver. In the worst case, the evasive maneuver does not allow braking anymore. We therefore introduce the duration of the evasive maneuver as GTTC, assuming no deceleration, and the lateral distance to fully reach an adjacent lane as $d_{\mathrm{eva}} > 0$.

Proposition 2 (Evasive Acceleration)
The required lateral acceleration a_{eva} of an evasive maneuver with initial lateral velocity $v_{\mathrm{lat}} \geq 0$ over the lateral distance d_{eva} with duration GTTC and reaction time for steering $\delta_{\mathrm{steer}} < \mathrm{GTTC}$ is obtained as

$$a_{\mathrm{eva}} = \frac{2\left(d_{\mathrm{eva}} - v_{\mathrm{lat}}(\mathrm{GTTC} - \delta_{\mathrm{steer}})\right)}{(\mathrm{GTTC} - \delta_{\mathrm{steer}})^2}.$$

Proof: The soundness of Prop. 2 has been shown in [41, III-A]. ∎

Based on the maximum possible acceleration $|a_{\mathrm{max}}|$, the maximum allowed deceleration is

$$a_{\mathrm{brake}} = \sqrt{a_{\mathrm{max}}^2 - a_{\mathrm{eva}}^2}. \quad (14)$$

In Step 5 of Fig. 3, the constraints on the vehicle's lateral motion are computed. Therefore, we predict the poses of the vehicle along Γ with respect to the previously planned longitudinal motion. Based on the approximation of the vehicle's shape described above (cf. Sec. III-B), the maximum allowed lateral offsets of each circle are computed, under the constraint that no collisions with obstacle occupanices occur. Let $\text{circ}_i(d, t)$ denote the occupancy of circle $i \in \{1, 2, 3\}$, which is shifted by d along the normal direction (note the sign of d) from the ego pose at time t. The maximum lateral offset constraints are

$$d_{i,\max}(t) = \sup \left\{ d \geq 0 \,\middle|\, \text{circ}_i(d, t) \cap \left(\bigcup_{b \in \mathcal{B}} \mathcal{O}_b(t) \right) = \emptyset \right\}. \tag{15}$$

The minimum lateral offset constraints $d_{i,\min}(t)$ are obtained analogously for negative values of d.

Note that if a circle initially intersects with an occupancy set for $d = 0$, the circle must be shifted to determine whether the ego vehicle should pass left or right. The passing side can be decided with reachability analysis, for example [42], and is not the focus of this work.

In Step 6, we check if $\exists t \in [0, t_h] : d_{\min}(t) > d_{\max}(t)$ which means that there is no longer a feasible solution because (9) has been violated. If the lateral planning problem becomes infeasible, we switch directly to the previously computed fail-safe trajectory which is still valid (cf. Fig. 1). However, if the evasive maneuver option is feasible, we plan the lateral motion of the ego vehicle as described in Sec. III-B and obtain the new valid fail-safe trajectory.

In contrast to existing verification methods, which do not return an alternative collision-free trajectory if the verification fails, our approach incorporates the verification in the planner by using over-approximative occupancy sets as constraints. If the utilized solver is numerically stable, the resulting fail-safe trajectory is guaranteed to be safe with respect to any physically feasible future motion of obstacles. The drivability of the trajectory considering controller uncertainties can be ensured using optimal control techniques, see e. g., [43].

V. EVALUATION

The longitudinal and lateral planners are implemented partly in *Python* and *C++* (for computational efficiency) on a computer with an Intel i5 1.4GHz processor and 8 GB of DDR3 1600 MHz memory. We use a discrete-time version of the vehicle models with step size Δt to construct the optimization by assuming a constant input for each discrete time step $k \in \{1, N\}$ over the time horizon t_h. We use the convex programming package *CVXPY* [15] and the solver *ECOS* [14].

Our scenarios are modeled using the *CommonRoad* benchmark suite for motion planning [44]. In order to predict the feasible future motion of obstacles, we use the open-source set-based prediction tool *SPOT* [38] and the motion assumptions listed in Tab. I. We set the maximum absolute acceleration of each vehicle to $|a_{\max}| = 8\,\mathrm{m\,s^{-2}}$ and the

TABLE I: List of motion assumptions based on [45].

Assumption	Description
A_{amax}	Maximum absolute accelerations $|a_{\max,b}| \geq |a_{\max,ego}|$ of traffic participants $b \in \mathcal{B}$ are known.
A_{vmax}	Positive longitudinal acceleration is stopped when a parameterized speed $v_{\max}$ is reached.
A_{back}	Driving backward in a lane is not allowed, i. e., $v \geq 0$.
A_{lane}	Changing lanes is only allowed if the new lane has the same driving direction.

vehicle dimensions to a length of $4.5\,\mathrm{m}$ and width of $2\,\mathrm{m}$. The parameters of the approximation of the ego vehicle's shape are $r = 1.3\,\mathrm{m}$ and $\ell = 3\,\mathrm{m}$.

We validated our approach on multiple CommonRoad scenarios and are able to compute fail-safe trajectories in less than $5\,\mathrm{ms}$ on average (cf. Tab. IV). A video showcasing different scenarios can be found in the video attachment of this paper and at https://mediatum.ub.tum.de/1453855.

A. Static Obstacle in Driveway

In our first scenario (cf. Fig. 5), the ego vehicle's driveway is blocked by a static obstacle b_1 (parameters listed in Tab. II). The ego vehicle is approaching the obstacle with a velocity of $v = 17\,\mathrm{m/s}$. Fig. 5a shows the last possible point at which the ego vehicle can perform a braking maneuver to avoid a collision with obstacle b_1. The occupancy of the ego vehicle along the braking trajectory is marked in red.

If the ego vehicle is closer to obstacle b_1 as illustrated in Fig. 5b, the only option to avoid a collision is to swerve to the left adjacent lane. However, if the vehicle is even closer to obstacle b_1, a collision cannot be avoided since the lateral acceleration and orientation constraints would be violated. Since the inputs are $\ddot{a}(t)$ for the longitudinal motion and $\ddot{\kappa}(t)$ for the lateral motion, the resulting fail-safe trajectories do not compromise comfort (cf. Fig. 5c) by minimizing jerks at the beginning.

B. Comparison with Sampling-based Planner

For comparison with another approach from the literature, we implemented a popular sampling-based trajectory planner that uses quintic polynomials to minimize jerk [7]. In contrast to our approach, quintic polynomials can only produce trajectories with a sigmoidal shape (cf. Fig. 5d). Depending on the complexity of the fail-safe maneuver, multiple replanning phases may be needed. For instance, in order to return to the initial lane in Fig. 5d, two consecutive trajectories need to be sampled. Determining the optimal time horizon t_h for the first trajectory part so that replanning is feasible may be challenging, e. g., we chose $t_h = 1.9\,\mathrm{s}$. In addition, discontinuities in the acceleration may arise when connecting trajectories as shown in [40].

Our approach directly obtains the optimal solution with global convergence, while sampling involves planning multiple trajectories and evaluating them with respect to potential collisions and costs, which increases the computation time.
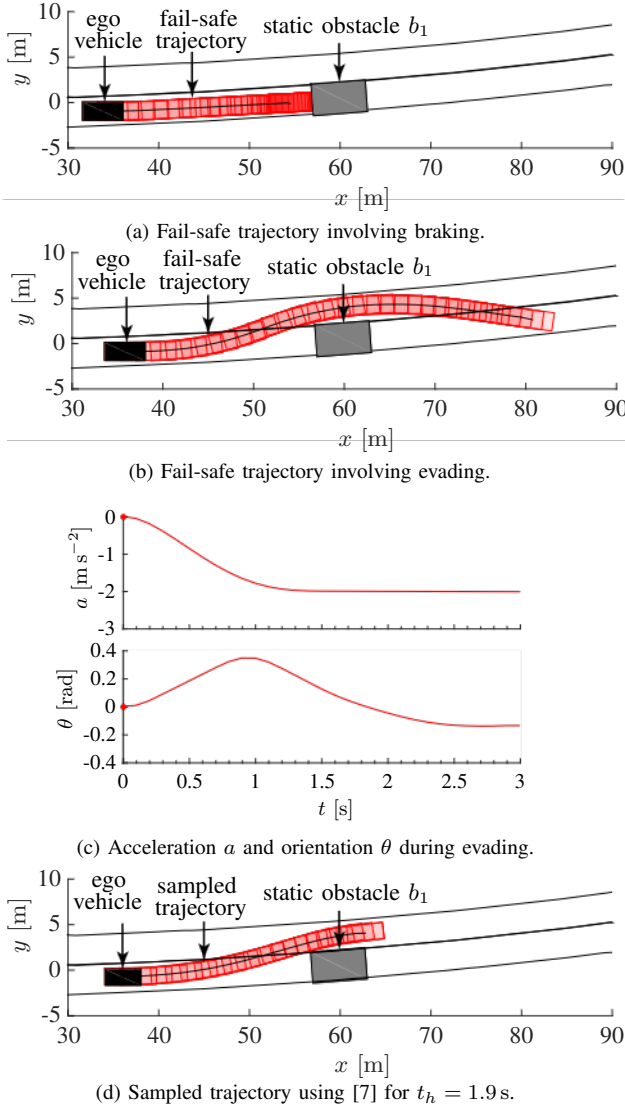
(a) Fail-safe trajectory involving braking.

(b) Fail-safe trajectory involving evading.

(c) Acceleration a and orientation θ during evading.

(d) Sampled trajectory using [7] for $t_h = 1.9\,\text{s}$.

Fig. 5: Scenario with a static obstacle b_1 which is blocking the lane of the ego vehicle. The ego vehicle can either brake (a) or perform an evasive maneuver (b) to avoid a collision (CommonRoad-ID: ZAM_Overtake-1_1:2018a). The acceleration a and orientation θ of the evasive maneuver are shown in (c). For comparison, we planned a trajectory using a sampling-based planner [7] in (d).

In our example, we sampled 3.9×10^3 candidate trajectories. Scenarios with more complexity may require the evaluation of even more candidates. Furthermore, planning in a discretized space is limited in that the only possible collision-free solution may be missed due to the used discretization step.

C. Urban T-junction

Let us now consider an urban environment (cf. Fig. 6a) in which the ego vehicle is approaching a T-junction along with three other vehicles b_i, $i \in \{1, 2, 3\}$ (parameters listed in Tab. III). The ego vehicle is driving with a speed of $v_0 = 8.3\,\text{m/s}$ and has the right of way on its lane; it can thus legally continue its intended motion if other vehicles give way.

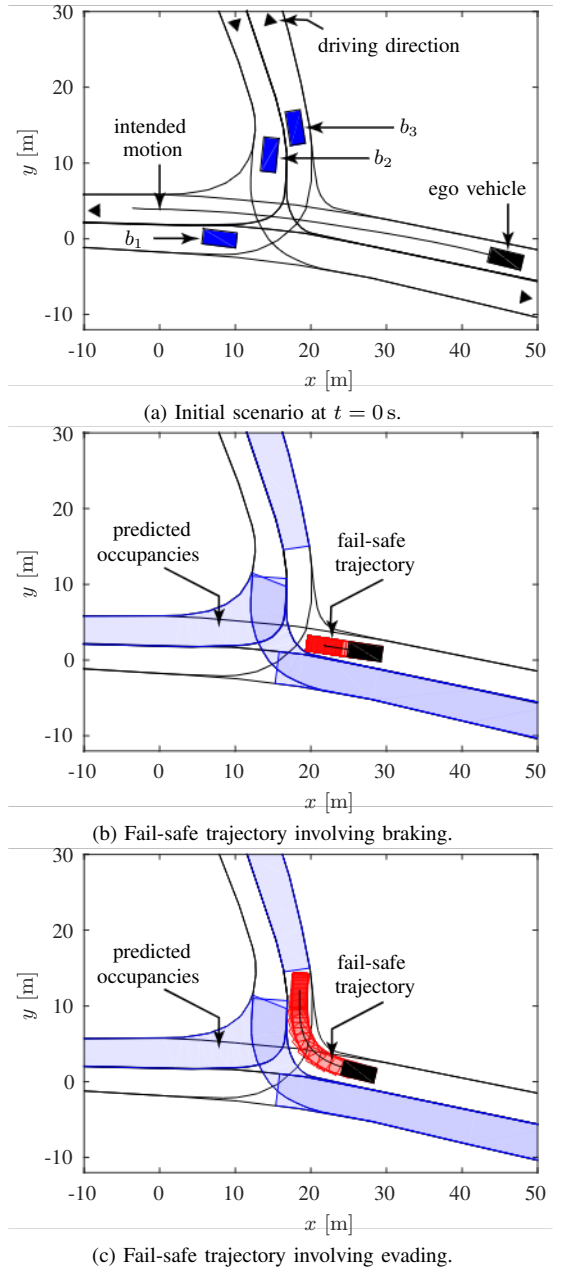Assuming vehicle b_2 disrespects the right-of-way rule, the

(a) Initial scenario at $t = 0\,\text{s}$.

(b) Fail-safe trajectory involving braking.

(c) Fail-safe trajectory involving evading.

Fig. 6: Urban T-junction scenario (CommonRoad-ID: DEU_Ffb-2_2_S-1:2018a) in which vehicle b_2 violates the right of way rule of the ego vehicle. The predicted occupancies are shown for $t = 6\,\text{s}$ for clarity. The ego vehicle can avoid a collision by emergency braking in (b) or using a combined braking and evasive maneuver to the right lane (c).

ego vehicle can remain safe with the fail-safe trajectory planned using our approach. Fig. 6b shows the pose of the last state along the intended motion of the ego vehicle from which a collision with the predicted occupancy of vehicle b_2 can be avoided with a braking maneuver. The ego occupancy along the planned fail-safe trajectory is marked in red.

After the ego vehicle has passed its last chance for braking along its intended motion, it can still avoid a collision by turning right and stopping behind vehicle b_3 as illustrated in Fig. 6c. Nevertheless, if the ego vehicle is too close to the occupied region, a collision cannot be avoided.

TABLE II: Parameters of the static obstacle scenario (cf. Sec. V-A).

Parameter	Description
Ego vehicle in (a)	$(x, y, \theta, v)_{\text{ego}}^{T} = (34\,\text{m}, -1\,\text{m}, 0\,\text{rad}, 17\,\text{m/s})^{T}$
Ego vehicle in (b)	$(x, y, \theta, v)_{\text{ego}}^{T} = (36\,\text{m}, -0.9\,\text{m}, 0\,\text{rad}, 17\,\text{m/s})^{T}$
Static obstacle b_1	$(x, y, \theta)_{\text{b1}}^{T} = (60\,\text{m}, -0.9\,\text{m}, 0.08\,\text{rad})^{T}$
Obstacle dimensions	length $= 6\,\text{m}$, width $= 3.5\,\text{m}$
Planning horizon	$t_h = 3.0\,\text{s}, N = 30, \Delta t = 0.1\,\text{s}$

TABLE III: Parameters of the urban T-junction scenario (cf. Sec. V-C).

Parameter	Description
Ego vehicle in (a)	$(x, y, \theta, v)_{\text{ego}}^{T} = (45.8\,\text{m}, -2.7\,\text{m}, 2.9\,\text{rad}, 8.3\,\text{m/s})^{T}$
Ego vehicle in (b)	$(x, y, \theta, v)_{\text{ego}}^{T} = (27.2\,\text{m}, 1\,\text{m}, 3\,\text{rad}, 8.3\,\text{m/s})^{T}$
Ego vehicle in (c)	$(x, y, \theta, v)_{\text{ego}}^{T} = (26.2\,\text{m}, 1.3\,\text{m}, 2.9\,\text{rad}, 8.3\,\text{m/s})^{T}$
Vehicle b_1	$(x, y, \theta, v)_{b_1}^{T} = (14.6\,\text{m}, 11\,\text{m}, -1.67\,\text{rad}, 7\,\text{m/s})^{T}$
Vehicle b_2	$(x, y, \theta, v)_{b_2}^{T} = (8\,\text{m}, 0\,\text{m}, -0.1\,\text{rad}, 14\,\text{m/s})^{T}$
Vehicle b_3	$(x, y, \theta, v)_{b_3}^{T} = (18\,\text{m}, 14.6\,\text{m}, 1.73\,\text{rad}, 7\,\text{m/s})^{T}$
Planning horizon	$t_h = 6.0\,\text{s}, N = 30, \Delta t = 0.2\,\text{s}$

TABLE IV: Average computation times of the longitudinal and lateral planners for each scenario.

| Scenario	Average computation time
Static obstacle	$t_{\text{lon}} = 1.2\,\text{ms}, t_{\text{lat}} = 2.9\,\text{ms}$
Urban T-junction	$t_{\text{lon}} = 0.8\,\text{ms}, t_{\text{lat}} = 3.2\,\text{ms}$
Highway scenario	$t_{\text{lon}} = 1.3\,\text{ms}, t_{\text{lat}} = 4.0\,\text{ms}$
Sampling planner [7]	$t = 510\,\text{ms}$

D. Cut-in Vehicle on Highway

In a third scenario, we demonstrate how our proposed approach enables the lateral planner to plan fail-safe maneuvers which let the ego vehicle swerve to another lane in order to avoid a collision. Therefore, we consider a highway scenario as illustrated in Fig. 7a, in which the ego vehicle is endangered by a cut-in of the slower driving vehicle b_1 (parameters listed in Tab. V).

If vehicle b_1 changes to the ego vehicle's lane, the ego vehicle cannot avoid a collision by solely braking. The utilized lateral collision constraints consider other obstacles and the left bound of the leftmost lane as well as the right bound of the shoulder lane. Considering these constraints, the solver is able to determine a feasible and collision-free fail-safe maneuver to the shoulder lane (cf. Fig. 7b).

VI. CONCLUSIONS

This paper develops a fail-safe trajectory planner for self-driving vehicles that employs a variational approach to compute fail-safe trajectories in arbitrary traffic scenarios.

In contrast to existing research on fail-safe maneuver planning, the trajectories are computed in real-time in continuous space by making use of convex optimization techniques for which mature and efficient solvers exist. In addition, our approach incorporates safety verification in the planner itself.
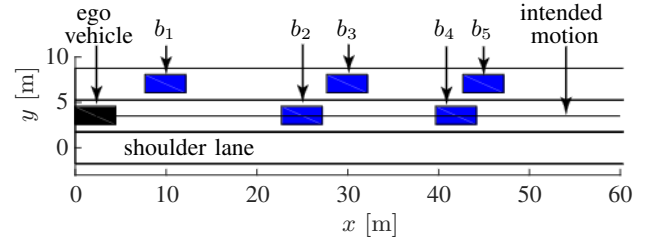
(a) Initial scenario at $t = 0\,\text{s}$.
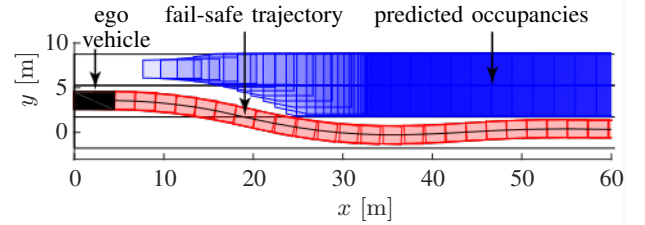
(b) Fail-safe trajectory involving swerving to the shoulder lane.

Fig. 7: Highway scenario (CommonRoad-ID: ZAM_HW-1_1_S-1:2018a) in which vehicle b_1 performs a cut-in to the ego vehicle's lane (a). The ego vehicle can avoid a collision by swerving to the adjacent shoulder lane (b). For clarity, the predicted occupancy is only shown for b_1.

TABLE V: Parameters of the highway scenario (cf. Sec. V-D).

Parameter	Description
Ego vehicle	$(x, y, \theta, v)_{\text{ego}}^{T} = (2.25\,\text{m}, 3.5\,\text{m}, 0\,\text{rad}, 23\,\text{m/s})^{T}$
Vehicle b_1	$(x, y, \theta, v)_{b_1}^{T} = (10\,\text{m}, 7\,\text{m}, 0\,\text{rad}, 20\,\text{m/s})^{T}$
Vehicle b_2	$(x, y, \theta, v)_{b_2}^{T} = (25\,\text{m}, 3.5\,\text{m}, 0\,\text{rad}, 25\,\text{m/s})^{T}$
Vehicle b_3	$(x, y, \theta, v)_{b_3}^{T} = (30\,\text{m}, 7\,\text{m}, 0\,\text{rad}, 30\,\text{m/s})^{T}$
Vehicle b_4	$(x, y, \theta, v)_{b_4}^{T} = (42\,\text{m}, 3.5\,\text{m}, 0\,\text{rad}, 20\,\text{m/s})^{T}$
Vehicle b_5	$(x, y, \theta, v)_{b_5}^{T} = (45\,\text{m}, 7\,\text{m}, 0\,\text{rad}, 35\,\text{m/s})^{T}$
Planning horizon	$t_h = 4.0\,\text{s}, N = 40, \Delta t = 0.1\,\text{s}$

Thus, the trajectories generated by the motion planner are always verified as safe. Simultaneously, our approach favors jerk-minimized fail-safe trajectories, which can enhance passenger comfort in case a critical situation suddenly resolves and the vehicle can return to the original intended motion.

We demonstrated the benefits of our comprehensive fail-safe planning approach in highway and urban scenarios and in comparison with a widely-used sampling based trajectory planner. We are currently implementing the approach in a test vehicle to gather real-world validation results.

ACKNOWLEDGMENTS

REFERENCES

[1] J. M. Anderson, N. Kalra, K. D. Stanley, P. Sorensen, C. Samaras, and O. A. Oluwatola, *Autonomous vehicle technology: a guide for policymakers*. RAND Corporation, 2014.

[2] S. Magdici and M. Althoff, "Fail-safe motion planning of autonomous vehicles," in *Proc. of the IEEE. Int. Conf. on Intelligent Transportation Systems*, 2016, pp. 452–458.

[3] B. Paden, M. Čáp, S. Z. Yong, D. Yershov, and E. Frazzoli, "A survey of motion planning and control techniques for self-driving urban vehicles," *IEEE Transactions on Intelligent Vehicles*, vol. 1, no. 1, pp. 33–55, 2016.

[4] S. M. LaValle and J. J. Kuffner, "Randomized kinodynamic planning," *Int. Journal of Robotics Research*, vol. 20, no. 5, pp. 378–400, 2001.

[5] S. Karaman and E. Frazzoli, "Sampling-based algorithms for optimal motion planning," *Int. Journal of Robotics Research*, vol. 30, no. 7, pp. 846–894, 2011.

[6] E. Frazzoli, M. A. Dahleh, and E. Feron, "Real-time motion planning for agile autonomous vehicles," in *Proc. of the American Control Conference*, 2001, pp. 43–49.

[7] M. Werling, J. Ziegler, S. Kammel, and S. Thrun, "Optimal trajectory generation for dynamic street scenarios in a Frenet frame," in *Proc. of the IEEE Int. Conf. on Robotics and Automation*, 2010, pp. 987–993.

[8] N. Ratliff, M. Zucker, J. A. Bagnell, and S. Srinivasa, "CHOMP: Gradient optimization techniques for efficient motion planning," in *Proc. of the IEEE Int. Conf. on Robotics and Automation*, 2009, pp. 489–494.

[9] D. Berenson, J. Kuffner, and H. Choset, "An optimization approach to planning for mobile manipulation," in *Proc. of the IEEE Int. Conf. on Robotics and Automation*, 2008, pp. 1187–1192.

[10] T. Schouwenaars, B. De Moor, E. Feron, and J. How, "Mixed integer programming for multi-vehicle path planning," in *Proc. of the IEEE European Control Conference*, 2001, pp. 2603–2608.

[11] J. Ziegler, P. Bender, T. Dang, and C. Stiller, "Trajectory planning for Bertha – a local, continuous method," in *Proc. of the IEEE Intelligent Vehicles Symposium*, 2014, pp. 450–457.

[12] D. Bertsekas, *Nonlinear Programming*, ser. Athena scientific optimization and computation series. Athena Scientific, 2016.

[13] S. P. Boyd and L. Vandenberghe, *Convex optimization*. Cambridge University Press, 2004.

[14] A. Domahidi, E. Chu, and S. Boyd, "ECOS: An SOCP solver for embedded systems," in *Proc. of the IEEE European Control Conference*, 2013, pp. 3071–3076.

[15] S. Diamond and S. Boyd, "CVXPY: A python-embedded modeling language for convex optimization," *The Journal of Machine Learning Research*, vol. 17, no. 1, pp. 2909–2913, 2016.

[16] P. Falcone, M. Tufo, F. Borrelli, J. Asgari, and H. E. Tseng, "A linear time varying model predictive control approach to the integrated vehicle dynamics control problem in autonomous systems," in *Proc. of the IEEE Int. Conf. on Decision and Control*, 2007, pp. 2980–2985.

[17] J. Nilsson, M. Ali, P. Falcone, and J. Sjöberg, "Predictive manoeuvre generation for automated driving," in *Proc. of the IEEE Int. Conf. on Intelligent Transportation Systems*, 2013, pp. 418–423.

[18] J. Nilsson, M. Brännström, J. Fredriksson, and E. Coelingh, "Longitudinal and lateral control for automated yielding maneuvers," *IEEE Transactions on Intelligent Transportation Systems*, vol. 17, no. 5, pp. 1404–1414, 2016.

[19] W. Zhan, J. Chen, C.-Y. Chan, C. Liu, and M. Tomizuka, "Spatially-partitioned environmental representation and planning architecture for on-road autonomous driving," in *Proc. of the IEEE Intelligent Vehicles Symposium*, 2017, pp. 632–639.

[20] B. Gutjahr, L. Gröll, and M. Werling, "Lateral vehicle trajectory optimization using constrained linear time-varying MPC," *IEEE Transactions on Intelligent Transportation Systems*, vol. 18, no. 6, pp. 1586–1595, 2016.

[21] T.-C. Au, C.-L. Fok, S. Vishwanath, C. Julien, and P. Stone, "Evasion planning for autonomous vehicles at intersections," in *Proc. of the IEEE Int. Conf. on Intelligent Robots and Systems*, 2012, pp. 1541–1546.

[22] K. Hirsch, J. Hilgert, W. Lalo, D. Schramm, and M. Hiller, "Optimization of emergency trajectories for autonomous vehicles with respect to linear vehicle dynamics," in *Proc. of the IEEE Int. Conf. on Advanced Intelligent Mechatronics*, 2005, pp. 528–533.

[23] C. Ackermann, J. Bechtloff, and R. Isermann, "Collision avoidance with combined braking and steering," *6th Int. Munich Chassis Symposium*, pp. 199–213, 2015.

[24] S. Bouraine, T. Fraichard, and H. Salhi, "Provably safe navigation for mobile robots with limited field-of-views in dynamic environments," in *Proc. of the IEEE Int. Conference on Robotics and Automation*, 2012, pp. 174–179.

[25] K. Macek, D. Vasquez, T. Fraichard, and R. Siegwart, "Towards safe vehicle navigation in dynamic urban scenarios," *Automatika*, vol. 50, no. 3-4, pp. 184–194, 2009.

[26] I. M. Mitchell, "Comparing forward and backward reachability as tools for safety analysis," in *Hybrid systems: computation and control*. Springer, 2007, pp. 428–443.

[27] M. Althoff and J. M. Dolan, "Online verification of automated road vehicles using reachability analysis," *IEEE Transactions on Robotics*, vol. 30, no. 4, pp. 903–918, 2014.

[28] S. L. Herbert, M. Chen, S. Han, S. Bansal, J. F. Fisac, and C. J. Tomlin, "FaSTrack: a modular framework for fast and guaranteed safe motion planning," in *Proc. of the IEEE Conference on Decision and Control*, 2017, pp. 1517–1522.

[29] P. Falcone, M. Ali, and J. Sjöberg, "Predictive threat assessment via reachability analysis and set invariance theory," *IEEE Transactions on Intelligent Transportation Systems*, vol. 12, no. 4, pp. 1352–1361, 2011.

[30] W. Damm, H.-J. Peter, J. Rakow, and B. Westphal, "Can we build it: formal synthesis of control strategies for cooperative driver assistance systems," *Mathematical Structures in Computer Science*, vol. 23, no. 04, pp. 676–725, 2013.

[31] M. Hilscher, S. Linker, and E.-R. Olderog, "Proving safety of traffic manoeuvres on country roads," in *Theories of Programming and Formal Methods*. Springer, 2013, pp. 196–212.

[32] S. Mitsch, S. M. Loos, and A. Platzer, "Towards formal verification of freeway traffic control," in *Proc. of the IEEE Int. Conf. on Cyber-Physical Systems*, 2012, pp. 171–180.

[33] T. Fraichard, "A short paper about motion safety," in *Proc. of the IEEE Int. Conf. on Robotics and Automation*, 2007, pp. 1140–1145.

[34] D. Althoff, J. J. Kuffner, D. Wollherr, and M. Buss, "Safety assessment of robot trajectories for navigation in uncertain and dynamic environments," *Autonomous Robots*, vol. 32, no. 3, pp. 285–302, 2012.

[35] D. Althoff, M. Althoff, and S. Scherer, "Online safety verification of trajectories for unmanned flight with offline computed robust invariant sets," in *Proc. of the IEEE Int. Conf. on Intelligent Robots and Systems*, 2015, pp. 3470–3477.

[36] K. Berntorp, A. Weiss, C. Danielson, and S. Di Cairano, "Automated driving: safe motion planning using positively invariant sets," in *Proc. of the IEEE Int. Conf. on Intelligent Transportation Systems*, 2017, pp. 1–6.

[37] S. Steyer, G. Tanzmeister, and D. Wollherr, "Grid-based environment estimation using evidential mapping and particle tracking," *IEEE Transactions on Intelligent Vehicles*, vol. 3, no. 3, pp. 384–396, 2018.

[38] M. Koschi and M. Althoff, "SPOT: A tool for set-based prediction of traffic participants," in *Proc. of the IEEE Intelligent Vehicles Symposium*, 2017, pp. 1686–1693.

[39] J. Ziegler and C. Stiller, "Fast collision checking for intelligent vehicle motion planning," in *Proc. of the IEEE Intelligent Vehicles Symposium*, 2010, pp. 518–522.

[40] C. Miller, C. Pek, and M. Althoff, "Efficient mixed-integer programming for longitudinal and lateral motion planning of autonomous vehicles," in *Proc. of the IEEE Intelligent Vehicles Symposium*, 2018, pp. 1954–1961.

[41] C. Pek, P. Zahn, and M. Althoff, "Verifying the safety of lane change maneuvers of self-driving vehicles based on formalized traffic rules," in *Proc. of the IEEE Intelligent Vehicles Symposium*, 2017, pp. 1477–1483.

[42] S. Söntges and M. Althoff, "Computing the drivable area of autonomous road vehicles in dynamic road scenes," *IEEE Transactions on Intelligent Transportation Systems*, pp. 1855 – 1866, 2017.

[43] B. Schürmann, D. Heß, J. Eilbrecht, O. Stursberg, F. Köster, and M. Althoff, "Ensuring Drivability of Planned Motions Using Formal Methods," in *Proc. of the IEEE Int. Conf. on Intelligent Transportation Systems*, 2017, pp. 1661–1668.

[44] M. Althoff, M. Koschi, and S. Manzinger, "CommonRoad: Composable benchmarks for motion planning on roads," in *Proc. of the IEEE Intelligent Vehicles Symposium*, 2017, pp. 719–726.

[45] Economic Comission for Europe: Inland Transport Committee, "Vienna Convention on Road Traffic," 1968. [Online]. Available: http://www.unece.org/fileadmin/DAM/trans/conventn/crt1968e.pdf